



# Afterpulse measurement of JUNO 20-inch PMTs

Rong Zhao<sup>1</sup> · Nikolay Anfimov<sup>2</sup> · Yu Chen<sup>1</sup> · Hang Hu<sup>1</sup> · Jun Hu<sup>3</sup> · Xiao-Lu Ji<sup>3</sup> · Denis Korablev<sup>2</sup> · Min Li<sup>3,4</sup> · Alexander Olshevskiy<sup>2</sup> · Zhao-Yuan Peng<sup>3</sup> · Arseny Rybnikov<sup>2</sup> · Zhong-Hua Qin<sup>3,5</sup> · Jun Wang<sup>1,6</sup> · Wei Wang<sup>1,6</sup> · Zhi-Min Wang<sup>3,4,7</sup> · Björn Wonsak<sup>8</sup>

Received: 18 July 2022 / Revised: 3 November 2022 / Accepted: 4 November 2022 / Published online: 30 January 2023

© The Author(s), under exclusive licence to China Science Publishing & Media Ltd. (Science Press), Shanghai Institute of Applied Physics, the Chinese Academy of Sciences, Chinese Nuclear Society 2023

## Abstract

In this study, we present the large photomultiplier tube (PMT) afterpulse measurement results obtained from the Jiangmen underground neutrino observatory (JUNO) experiment. A total of 11 dynode-PMTs (R12860) from the Hamamatsu company (Hamamatsu Photonics K.K. (HPK)) and 150 micro-channel plate PMTs (MCP-PMTs, GDB-6201) from the NNVN company (North Night Vision Technology Co., Ltd. (NNVT)) were tested. Subsequently, an afterpulse model was built according to the afterpulse time distribution and the probability of occurrence for these two types of PMTs. The average ratio of the total afterpulse charge with a delay between 0.5  $\mu$ s and 20  $\mu$ s to the primary pulse charge is  $\sim 5.7\%$  (13.2%) for the tested MCP-PMTs (dynode-PMTs). The JUNO experiment will deploy 20,012 20-inch PMTs; this study will benefit detector simulation, event reconstruction, and data analysis regarding the JUNO experiment.

**Keywords** Afterpulse · MCP-PMT · JUNO · Dynode-PMT · 20-inch PMT

This work was supported by Strategic Priority Research Program of the Chinese Academy of Sciences (No. XDA10011100), Joint Institute of Nuclear Research (JINR), Russia and Lomonosov Moscow State University in Russia, joint Russian Science Foundation (RSF), DFG (Deutsche Forschungsgemeinschaft), and National Natural Science Foundation of China (Nos. 12090062 and 12075087). The authors acknowledge all their colleagues from the JUNO collaboration who operated the 20-inch PMT testing system.

✉ Wei Wang  
wangw223@mail.sysu.edu.cn

Yu Chen  
cheny73@mail.sysu.edu.cn

<sup>1</sup> School of Physics, Sun Yat-sen University, Guangzhou 510275, China

<sup>2</sup> Joint Institute for Nuclear Research, Dubna 141980, Russia

<sup>3</sup> Institute of High Energy Physics, Chinese Academy of Sciences, Beijing 100049, China

<sup>4</sup> University of Chinese Academy of Sciences, Beijing 100049, China

## 1 Introduction

Jiangmen underground neutrino observatory (JUNO) is a reactor anti-neutrino experiment designed with multiple physical goals, including determining the mass ordering of neutrinos and high-precision measurements of neutrino oscillation parameters [1–3]. Central Detector (CD) of JUNO is a Liquid Scintillator (LS) detector with 20 ktons LS enclosed in an acrylic sphere with a diameter of 35.4 m. Ultrapure water will be filled outside the acrylic sphere in the water pool. There will be 17,612 20-inch photomultiplier tubes (PMTs) viewing photons generated in CD volumes,

<sup>5</sup> State Key Laboratory of Particle Detection and Electronics, Beijing 100049, China

<sup>6</sup> Sino-French Institute of Nuclear Engineering and Technology, Sun Yat-sen University, Zhuhai 519082, China

<sup>7</sup> State Key Laboratory of Particle Detection and Electronic, Beijing 100049, China

<sup>8</sup> Institut für Experimentalphysik, Universität Hamburg, Hamburg 20148, Germany

comprising 5,000 dynode-PMTs and 12,612 micro-channel plate PMTs (MCP-PMTs) [1, 2]. Additionally, 2,400 20-inch PMTs were positioned in the water pool veto system. The pulses generated by 20-inch PMTs for one event will be used to reconstruct the information about the detected particles [4–6].

Afterpulses are undesired signals that follow the light-induced photoelectron signal (called the primary pulse) of PMTs. Its mechanism has been studied for a long time and is known to have a negative effect on the timing of the PMTs [7–13]. Afterpulses are mainly caused by positive ions emitted from the ionization of residual gases inside the PMTs [7], which are difficult to distinguish from the actual light-induced signal. The afterpulse signals mimic the signal and worsen the PMT time resolution, thereby affecting the particle identification and event reconstruction in the JUNO experiment. Consequently, the JUNO experiment requires the total afterpulse ratio to be less than 15% for 20-inch PMTs [1]. The 20-inch dynode-PMTs manufactured by HPK use traditional dynodes as an electron multiplication system, and there have been many afterpulse testing results for this type of PMTs [14, 15]. However, the afterpulse characteristics of newly developed 20-inch MCP-PMTs are not well understood because of MCP's special electron multiplication mechanism [16]. In this study, we focus on ion-initiated afterpulses that occur hundreds of nanoseconds after the primary pulse, while light-induced late pulses (arising from photoelectron backscattering) are not covered [17–20]. The afterpulse measurement is part of JUNO's PMT characterization test from 2017 to 2021, during which 150 MCP-PMTs and 11 dynode-PMTs were sampled for afterpulse measurement. The testing data and operational notes were managed using the JUNO PMT testing database [21]. Section 2 describes the experimental setup and waveform data analysis, and Sect. 3 describes the time and charge distribution of afterpulses and a simplified afterpulse model of JUNO PMTs.

## 2 Experiment setup and afterpulse testing method

### 2.1 Experiment setup

The JUNO PMT instrumentation group built two independent testing systems for the performance characterization of 20-inch PMTs: The scanning station, which is designed for precise PMT photocathode characterization [22, 24], and a container system that is appropriate for PMT mass testing [23, 24]. Both facilities were capable of measuring afterpulse signals of 20-inch PMTs.

A block diagram of the measurement equipment at the scanning station is presented in Fig. 1. During each

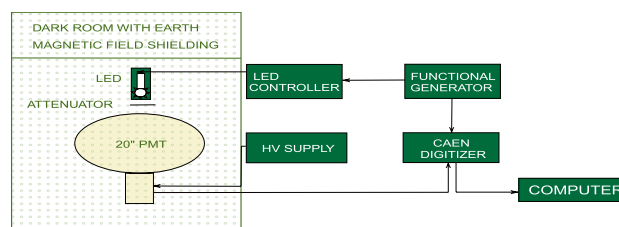
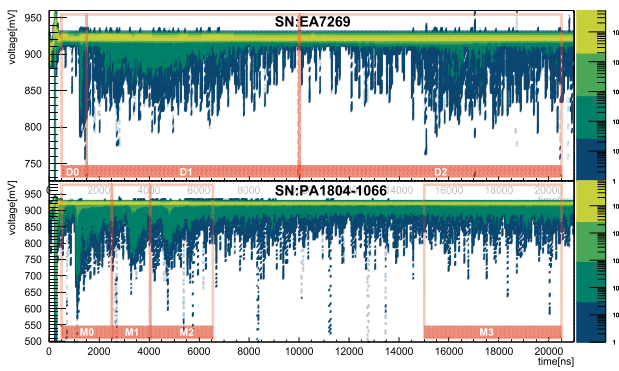


Fig. 1 Schematic overview of the testing system in scanning station

afterpulse test, the tested PMTs were installed by an aluminum holder and connected to the JUNO official PMT base [1]. The PMT base provides a positive high voltage (HV) to PMT and couples the PMT signal to a waveform digitizer. A 10-bits fast ADC (analog-to-digital converter, CAEN VME1751) was used for waveform digitization. A 420-nm light-emitting diode (LED) was mounted immediately above the PMT, and absorptive ND filter from ThorLab was mounted between the LED and PMT to attenuate the light intensity [25]. The LED has an internal light intensity monitoring and feedback control system to achieve a 1% level of intensity stability. The light intensity can be adjusted using an LED controller from 0 photoelectrons (p.e.) to hundreds of photoelectrons per pulse during one afterpulse measurement. External trigger signals from the pulse generator were used to trigger the LED and digitizer at a frequency of 100 Hz. A previous study has shown that large-size PMTs are sensitive to the Earth's magnetic field (EMF) owing to its influence on the motion of electrons inside the PMT [26]. To avoid the influence of EMF, a dark room was designed with an Earth magnetic field shielding function using three independent groups of Helmholtz coils [22]. The residual EMF can achieve a 0.5  $\mu\text{T}$  level ( $\sim 1/10$  of the local EMF intensity) at the center of the dark room where the PMT is mounted.

The container #4 system adopted JUNO electronics for waveform digitization [1], which can capture a 10  $\mu\text{s}$ -long PMT waveform frame. Instead of using LED as the light source, the container electronics operate in the self-trigger mode for the afterpulse measurements. A relatively large trigger threshold (with an amplitude approximately 15 times higher than a single p.e.) was used to select events with large primary signals. The possible sources of these large signals (serving as the primary pulse in the afterpulse measurement) in the dark environment could be cosmic rays, radioactive background, etc. [27]. The container afterpulse measurement has independent light source and electronics with the scanning station and thus can double-check the afterpulse timing results.



**Fig. 2** (Color online) The two-dimensional contour plot constructed by stacking 20,000 tested raw waveform frames. The top panel is from one dynode-PMT with SN “EA7269”, and bottom panel is from one MCP-PMT with SN “PA1804-1066”

### 2.2 Afterpulse test method

It has been confirmed that the afterpulse rate and charge depend on primary pulse intensity [8, 29]. Accordingly, for each afterpulse test, we used three different light intensities with average intensities of ~ 40 p.e., ~ 80 p.e., and ~ 120 p.e. to evaluate the final afterpulse level of PMTs. In addition, another test under the same condition but LED turned off is performed to evaluate and subtract the contribution from PMT dark count signals. During one afterpulse measurement, the electronics of the scanning station recorded ~ 20,000 waveform frames (21 μs period) for each LED light intensity.

As shown in Fig. 2, the two-dimensional contour plot obtained by stacking all 20,000 waveform frames from one measurement displays the general characteristics of afterpulse signals such as time and amplitude distributions. The bottom panel of Fig. 2 shows the afterpulse measurement results from one MCP-PMT with serial number (SN) “PA1804-1066”. For this PMT, the primary pulse signals arrive at approximately 300 ns, and three afterpulse signal groups (arriving at ~ 1.2 μs, 3.7 μs, and 5 μs) can be clearly identified. The top panel of Fig. 2 shows the test results of a dynode-PMT (SN: “EA7269”). The primary pulse signals at ~ 300 ns and afterpulse signals can be identified at ~ 1 μs, ~ 4.5 μs, and 15 μs.

The pulses generated by LED light injection are marked as primary pulses. The pulses arrive 500 ns after the primary pulse are marked as afterpulses. Some previous afterpulse measurements of the 8-inch PMT demonstrated that

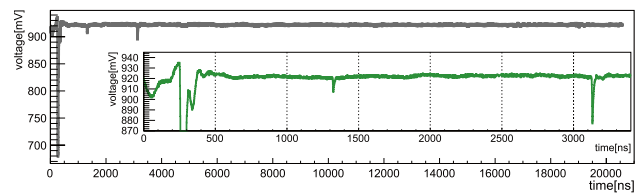


**Fig. 3** A tested waveform with 21 μs length

the  $H_2^+$ -induced afterpulse arrival time is ~ 200 ns, and this time delay is the shortest compared to the time delay of afterpulses caused by other ions [9, 10, 30]. For the 20-inch PMTs, the drift time of ions is much longer than that of the 8-inch PMTs. It is reasonable to address the first group of afterpulses (with a time delay of approximately 900 ns) to an  $H_2^+$ -induced afterpulse [8, 9, 29, 31–33]. The pulses after the primary pulse but with a time delay of less than 500 ns (late pulses) were ignored in this study because they are not generated by residual ions.

Afterpulses of different populations are caused by ions with different time delays; therefore, it is convenient to divide them into groups according to their different time delays. Four groups of afterpulse are confirmed for 20-inch MCP-PMTs, tagged M0, M1, M2 and M3; three groups of afterpulse are confirmed for 20-inch dynode-PMTs, tagged D0, D1, and D2. The time windows for the searching of these afterpulses in data analysis are summarized in Table 1.

The method to classify afterpulses into groups by their arrival time is not perfect because, in one time window, there could be multiple sources of afterpulses with different amplitudes or charge distributions but with similar time delays [9]. In this study, we only focused on the dominant afterpulse signals in one selected time window and ignored the non-significant components that may occur when a much higher HV is applied to PMTs.

### 2.3 Afterpulse waveform analysis

Figure 3 shows a typical single waveform captured for afterpulse analysis. The primary pulse arrives at approximately 280 ns on the time axis; subsequently, two afterpulse signals appear at ~ 1300 ns and ~ 3100 ns. In the zoom-in section of Fig. 3, it is shown that the baseline around primary pulse is distorted by the pre-pulses, late pulses, and potential EM noise [18]. Therefore, the baseline of primary pulse is

**Table 1** The time windows of different afterpulse signal groups

PMT model	MCP-PMT				Dynode-PMT		
	M0	M1	M2	M3	D0	D1	D2
Afterpulse group	M0	M1	M2	M3	D0	D1	D2
Searching region start (ns)	500	2500	4000	15000	500	1500	10000
Searching region end (ns)	2500	4000	7000	20500	1500	10000	20500

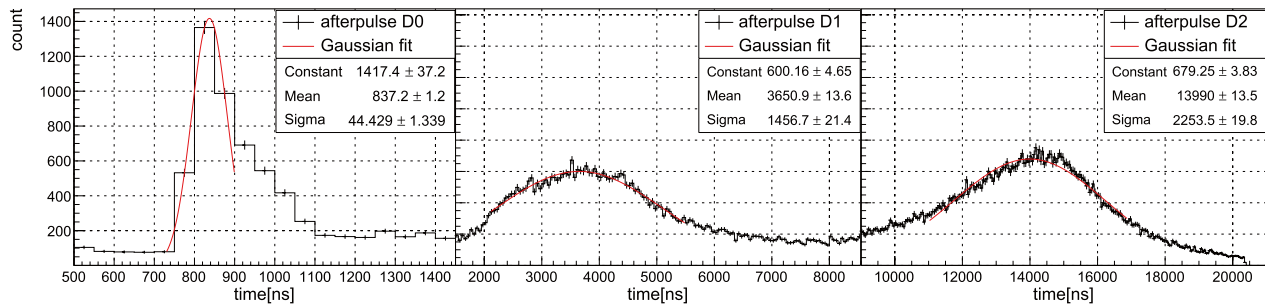


**Fig. 4** Gaussian fitting of afterpulse time distribution for one dynode-PMT, SN: “EA7217”

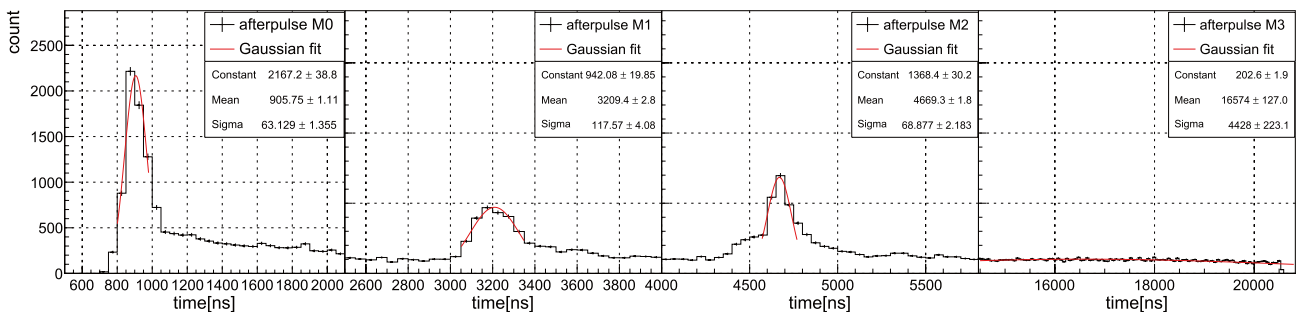


**Fig. 5** Gaussian fitting of afterpulse time distribution for one MCP-PMT, SN: “PA1906-2539”

calculated as the mean value of waveform from 10  $\mu\text{s}$  to 20  $\mu\text{s}$  where the waveform is less affected by LED induced signals. The charge of the primary pulse (afterpulse) is integrated from  $-25$  ns to  $+50$  ns from the peak position of the primary pulse (afterpulse). A 3 mV threshold is used to seek afterpulse signals; the charge of one afterpulse signal must be larger than 0.25 single p.e. charge to exclude negligible signals or low-frequency noise.

For each primary pulse, all afterpulse signals in the time range  $[T_{pp}+500, 21000]$  ns were recorded for analysis, where  $T_{pp}$  is the arrival time of the primary pulse. For the baseline calculation of afterpulses, we used the average value over a 50 ns time interval before the threshold-cross time of one afterpulse signal. The arrival time of one afterpulse (primary pulse) signal  $T_{AP}$  ( $T_{pp}$ ) was calculated based on the threshold-cross time of its leading edge. If one afterpulse is detected at  $T_i$ , we search for the next afterpulse from  $T_i + 50$  ns. Accordingly, the minimum time interval between two adjacent afterpulses belonging to one primary pulse is 50 ns in this study.

### 3 Afterpulse characterization results

The timing features and charge distribution of the afterpulse signals are two of the most critical parameters for the afterpulse measurements in JUNO 20-inch PMTs. Previous studies have demonstrated that both the charge and rate of the afterpulse depend on the primary pulse intensity, HV (gain) of the PMT, and EMF shielding [22]. Before each afterpulse test, the working HV of one candidate PMT is tuned to achieve PMT a gain<sup>1</sup> of  $G = 10^7$ , which is limited within the range  $[0.95 \times 10^7, 1.05 \times 10^7]$ . Then, for each PMT test, the EMF shielding is turned on and three different LED light intensities are applied to characterize the afterpulses.

#### 3.1 Timing of afterpulse signals

The afterpulse time is defined as the delay between one afterpulse signal and its corresponding primary pulse signal,  $t_{AP} = T_{AP} - T_{pp}$ , where  $T_{AP}$  ( $T_{pp}$ ) denotes the arrival time of afterpulse (primary pulse). For one PMT, the afterpulse time of each waveform is filled into a histogram and then fitted

<sup>1</sup> MCP-PMT’s typical working HV is approximately 1750 V and dynode-PMT’s HV is approximately 1820 V.

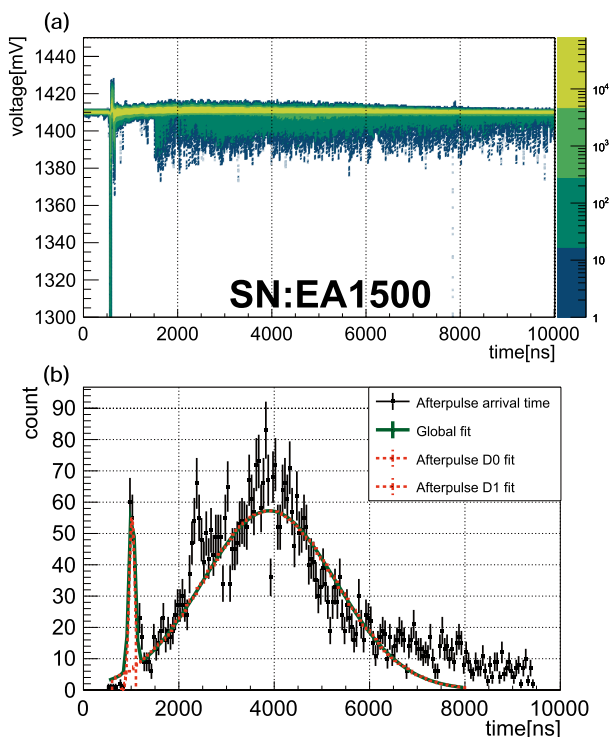


**Fig. 6** (Color online) The two-dimensional waveform stacking contour histogram of dynode-PMT “EA1500” (top panel) and histogram of afterpulse arrival time ( $t_{AP}$ ) distribution (bottom panel), measured using the container system

using a Gaussian function. Accordingly, the fitted mean value  $t_{AP}^i$  is referred to as the time for a group  $i$  ( $i = D0, D1, \dots$ ) of afterpulses.

The afterpulse time distribution histograms and fitting results of one dynode-PMT (SN: “EA7217”) are plotted in Fig. 4; the afterpulse time distribution histograms and fitting results of one MCP-PMT (SN: “PA1906-2539”) are plotted in Fig. 5. For the MCP-PMT, the fitted afterpulse times of M0, M1, M2, and M3 are  $t_{AP}^{M0} = 906 \pm 1$  ns,  $t_{AP}^{M1} = 3209 \pm 3$  ns,  $t_{AP}^{M2} = 4669 \pm 2$  ns, and  $t_{AP}^{M3} = 16.57 \pm 0.13$   $\mu$ s, respectively. For the dynode-PMT, the fitted afterpulse times of D0, D1, and D2 are  $t_{AP}^{D0} = 837 \pm 1$  ns,  $t_{AP}^{D1} = 3651 \pm 14$  ns, and  $t_{AP}^{D2} = 13990 \pm 14$  ns, respectively. The uncertainty of  $t_{AP}^i$  is estimated considering both the contribution from the primary pulse and afterpulse.

As mentioned in Sect. 2, the container #4 PMT test system is also used for the afterpulse timing study to cross-check the scanning station measurement. Owing to the limitation of the hardware configuration, the electronics of the container #4 system can only record a 10  $\mu$ s long waveform for afterpulse measurement [28]. Figures 6 and 7 plot the testing results for one dynode-PMT and one MCP-PMT, respectively, obtained using the container system. The top panel is a two-dimensional stacking contour plot of 20,000

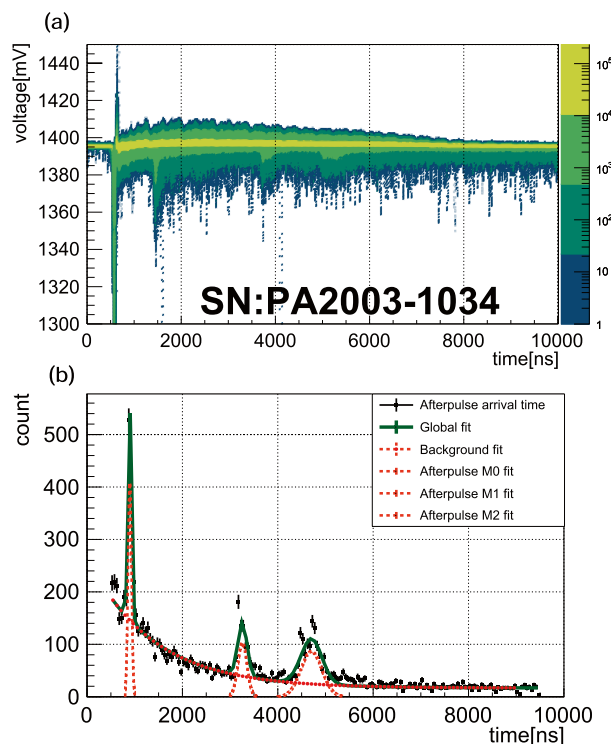


**Fig. 7** (Color online) The two-dimensional waveform stacking contour histogram of MCP-PMT “PA2003-1034” (top panel) and histogram of afterpulse arrival time ( $t_{AP}$ ) distribution (bottom panel), measured using the container system

waveform frames, and the bottom panel is the histogram of the afterpulse time distribution and fitting results. There is some extra noise in the self-trigger mode afterpulse measurement of the MCP-PMTs. This type of signal-induced pulse starts near the end of the primary pulse signal and is distributed exponentially.

An exponential background and three Gaussian functions were used to achieve a global fitting of the afterpulse time histogram for the MCP-PMT; two Gaussian functions were used to fit the afterpulse time histogram of the dynode-PMT. For MCP-PMT (“PA2003-1034”), the fitted afterpulse time of M0, M1, and M2 are  $896 \pm 2$  ns,  $3259 \pm 8$  ns, and  $4705 \pm 9$  ns, respectively; for dynode-PMT (“EA1500”), the afterpulse time of D0 (D1) is  $1018 \pm 8$  ns ( $3879 \pm 26$  ns).

The results obtained from the scanning station and container system confirmed the timing features of the three groups of MCP-PMT’s afterpulse and two groups of dynode-PMT’s afterpulse. These two PMT testing systems have independent light sources and electronics and thus can exclude potential flaws in light sources or electronics problems.

The afterpulse timing features of JUNO 20-inch dynode-PMTs are similar to the results obtained with smaller

**Table 2** The arrival time of each group of afterpulse averaged over all the tested PMTs

PMT Model	MCP-PMT				dynode-PMT		
Afterpulse group	M0	M1	M2	M3	D0	D1	D2
$\bar{t}_{AP}^i$ (ns)	910	3134	4579	17731	1067	4239	15081
Uncertainty of $\bar{t}_{AP}^i$ (ns)	14	61	87	600	132	1957	2791

dynode-PMTs [10, 11]; the afterpulse timing results of MCP-PMTs are consistent with data published by vendors [35]. For each afterpulse component, a weighted average over all tested PMTs (150 MCP-PMTs and 11 dynode-PMTs) is calculated as the final afterpulse delay time  $\bar{t}_{AP}^i$  and their uncertainties are listed in Table 2.

### 3.2 Charge distribution of afterpulse signals

Afterpulses with different time delays are caused by different types of ions, each of which having a different capability of generating secondary electrons from the photocathode.

Figure 8 plots the typical charge distribution of each group of afterpulse when the primary pulse light intensity is  $\sim 120$  photoelectrons. The top panel is obtained from one MCP-PMT (SN: “PA1804-1066”), while the bottom panel is obtained from one dynode-PMT (SN: “EA7269”). The afterpulse charge of each event is normalized to the primary pulse charge with 100 photoelectrons in the histograms, assuming that the afterpulses’ charge is proportional to the charge of the primary pulse.

The charge distribution histograms of MCP-PMT show that afterpulse M0 contains more average photoelectrons than the others, which could be a feature of hydrogen-induced afterpulses [30].

The charges of afterpulses M1 and M2 are approximately at the level of tens of photoelectrons; however, most of the M3 afterpulses are single p.e. signals. For dynode-PMT, afterpulse D0 has more average photoelectrons than the others; D1 and D2 mostly contain single photoelectron signals. Comparing the results of the MCP-PMT and dynode-PMT in Fig. 8a-b, we observe that the afterpulse charges of dynode-PMT are less than 25 photoelectrons when the PMT is illuminated by a primary pulse of 100 photoelectrons, while afterpulses of MCP-PMT have more average photoelectrons for each event. The difference in afterpulse charge (time) distribution between these two types of PMTs is related to their different photocathode materials, geometry design, and electron multiplication mechanisms. A detailed discussion about the charge response of MCP-PMT and dynode-PMT can be found in Ref. [34].

The charge distributions of different groups of afterpulses when the PMT is illuminated by different LED intensities are shown in Figs. 9a–c and 10a–d. For both dynode-PMT and MCP-PMT, the total afterpulse rate (with dark count rate removed) of all afterpulse components grows with a

higher primary pulse intensity, which is consistent with the results obtained in previous studies [11, 31, 35, 36].

The afterpulse charge distribution and dependency of afterpulse rate on the primary pulse charge vary for different afterpulse groups. Subsequently, the total charge ratio between all afterpulses and primary pulse is defined to describe the total afterpulse level for JUNO 20-inch PMTs.

### 3.3 Afterpulse model of 20-inch JUNO PMTs

The charge and arrival time distributions of afterpulses from all the tested PMTs are plotted in two-dimensional contour plots, as shown in Fig. 11a–b (with a primary pulse  $\sim 120$  p.e.). Because all the PMTs were

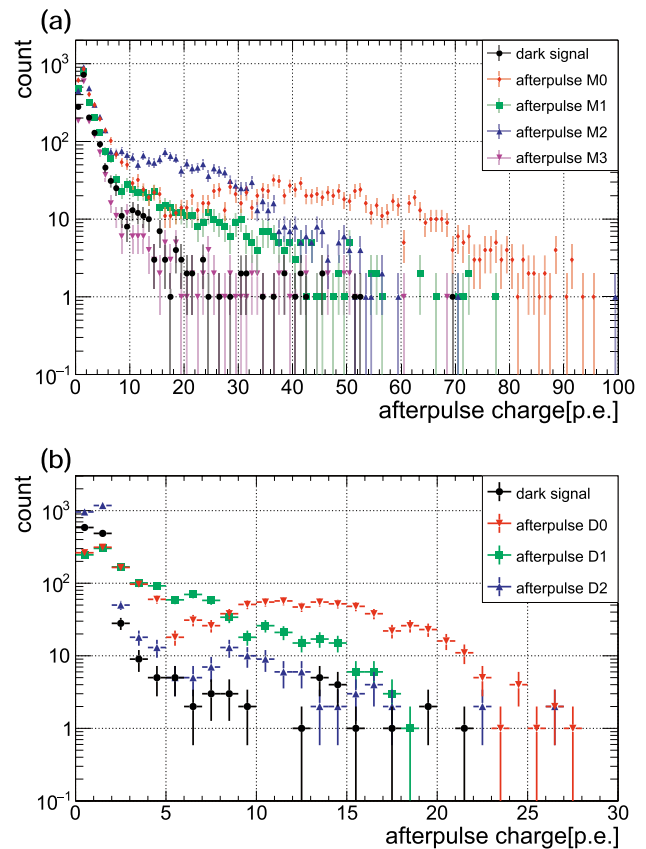


**Fig. 8** (Color online) Charge distribution of different afterpulse groups in a number of photoelectrons, the primary pulse intensity is  $\sim 120$  photoelectrons. Top panel: MCP-PMT. Bottom panel: dynode-PMT

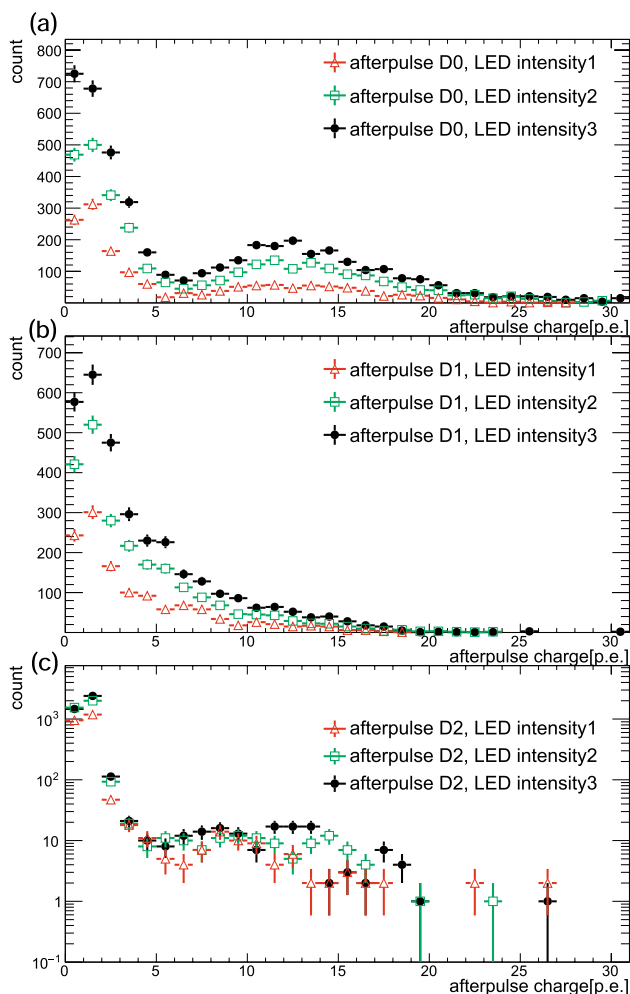


**Fig. 9** (Color online) Charge distribution of different group of afterpulses of one dynode-PMT “EA7269” in number of photoelectrons, the three LED intensities are plotted in different colors. The primary pulse intensity corresponding to light intensity 1 (2, 3) is 19.1 (43.7, 68.9) photoelectrons

manufactured using the same technology, the afterpulse timing features are preserved even after the averaging process. Four (three) groups of afterpulse signals of MCP-PMTs (dynode-PMTs) can still be identified.

For one PMT, the charge ratio of group  $i$  afterpulse  $R_{AP}^i$  is defined as follows:

$$R_{AP}^i = \frac{\sum_j Q_{AP}^{ij} - Q_{dark}^i}{\sum_j Q_{PP}^{ij}}, \tag{1}$$

where  $Q_{AP}^{ij}$  denotes the total charge of group  $i$  afterpulse signal in frame  $j$  and  $Q_{PP}^{ij}$  denotes the charge of the primary pulse signal in frame  $j$ .  $Q_{dark}^i$  denotes the total charge contribution from the dark signal in the time window of the afterpulse group  $i$ . Subsequently,  $Q_{dark}^i$  is calculated as

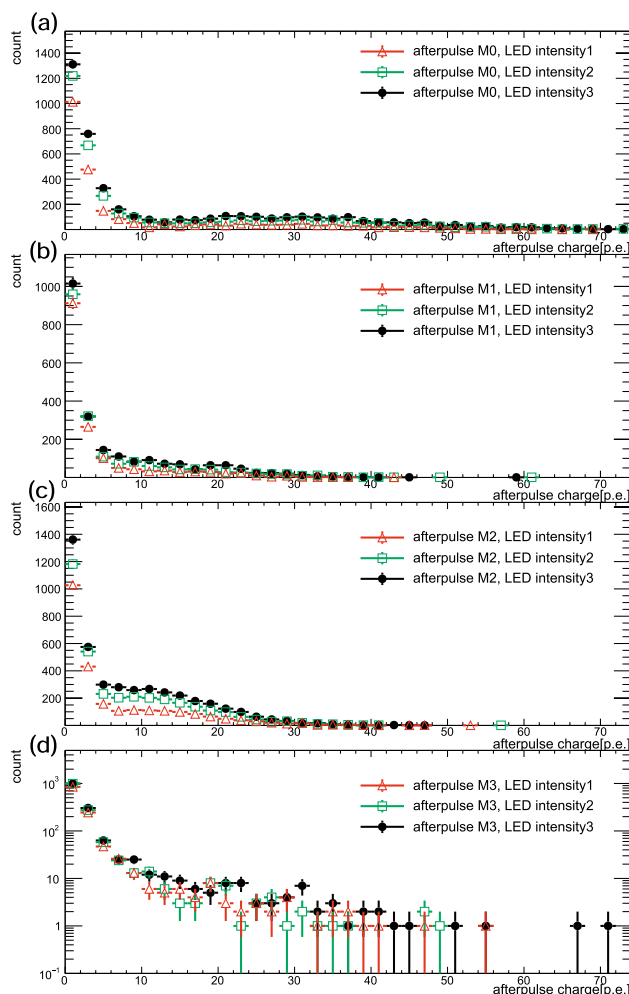


**Fig. 10** (Color online) Charge distribution of different afterpulse groups for one MCP-PMT “PA1808-2151” in number of photoelectrons; the three LED intensities are plotted in different colors. The primary pulse intensity corresponding to light intensity 1 (2, 3) is 39.7 (84.1, 128.2) photoelectrons

$Q_{dark}^i = \sum_j \frac{w_i}{W} Q_{dark}^j$ , where  $Q_{dark}^j$  is the total charge for frame  $j$  in the dark test,  $w_i$  is the width of the selection time window for afterpulse group  $i$  and  $W$  is the total length of the wave frame. Then, the total charge ratio  $R_{AP}$  of one tested PMT is defined as the sum of all afterpulse components,

$$R_{AP} = \sum_i R_{AP}^i. \tag{2}$$

For one PMT,  $R_{AP}$  represents the ratio of the total charge induced by afterpulses to the total charge induced by the primary pulses. This value  $R_{AP}$  is treated as the afterpulse occurrence probability of one PMT. The afterpulse charge ratio of each afterpulse group and total charge ratio  $R_{AP}$  are averaged over all the tested PMTs, which are summarized in Table 3.

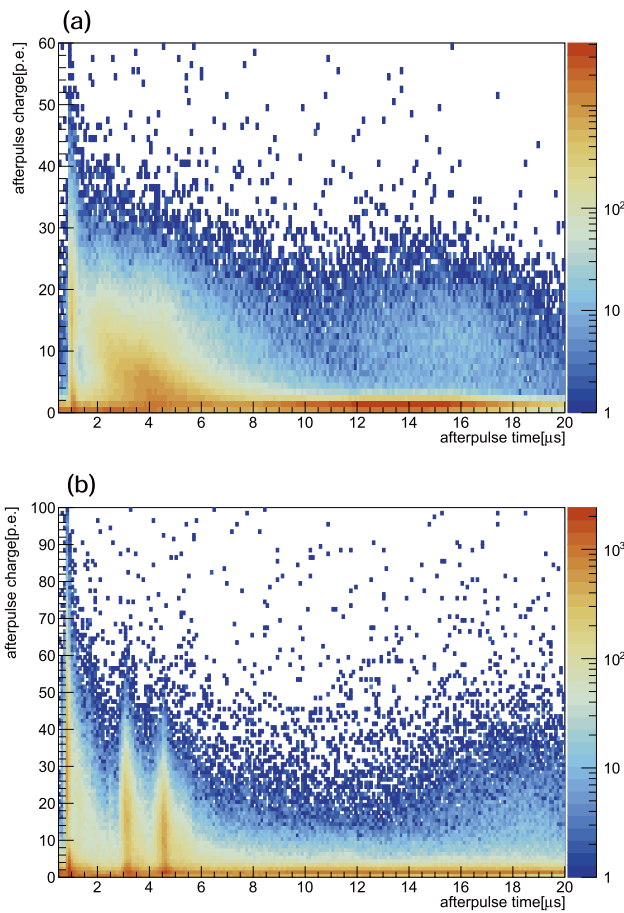


**Fig. 11** (Color online) The two-dimensional contour plot of the charge-time ( $t_{AP}$ ) distribution of afterpulses for dynode-PMTs (top panel) and MCP-PMTs (bottom panel) with light intensity 120 p.e. per trigger

The stability of the LED light intensity, afterpulse searching threshold, and dark count of PMT are considered when calculating the systematics. The uncertainties of the charge ratio calculation are estimated considering both the experimental and statistical errors using conservative values.

A simplified afterpulse model can be built for JUNO 20-inch PMTs based on the afterpulse testing data with the following two assumptions: only the dominant components of afterpulse in one time region are considered,

and the total charge ratio between afterpulses and primary pulse is calculated as the probability of occurrence for each afterpulse component. In this model, the afterpulse time distribution is described by a Gaussian function; the corresponding charge probability is a coefficient, as shown in Eq. (3) and Eq. (4):

$$P_{AP}^{MCP-PMT} = 0.019 \times G(0.91, 0.069) + 0.016 \times G(3.134, 0.154) + 0.018 \times G(4.579, 0.125) + 0.007 \times G(17.731, 3.896), \tag{3}$$

$$P_{AP}^{dynode-PMT} = 0.007 \times G(1.067, 0.075) + 0.065 \times G(4.239, 1.312) + 0.06 \times G(15.081, 2.602), \tag{4}$$

where  $G(\mu, \sigma) = \frac{1}{\sigma\sqrt{2\pi}} \cdot \exp\left(-\frac{(t-\mu)^2}{2\sigma^2}\right)$  denotes a normal distribution. The coefficient before each Gaussian function denotes the occurrence probability of one afterpulse component when there is a primary pulse with a charge of 1 p.e.,  $\mu$  denotes the average time of one group of afterpulses, and  $\sigma$  denotes the standard deviation of the time distribution of one afterpulse component. Considering all the confirmed afterpulse components, the final afterpulse charge ratio of the JUNO MCP-PMT (dynode-PMT) is 5.7% (13.2%), which is consistent with previous measurements [35–37].

The afterpulse model defined in Eqs. (3) and (4) is based on testing data with a primary pulse intensity of 100 p.e.. It is not clear whether this model still works when the primary pulse is several p.e. levels because the dependency of afterpulse charge and rate on primary charge intensity could be different at very low primary pulse intensity owing to the complex structure and manufacturing technology of these large-size PMTs [7, 9, 11, 35, 37].

### 4 Conclusion and discussion

In total, 150 MCP-PMTs and 11 dynode-PMTs were tested to study the afterpulse timing and charge characteristics of the JUNO 20-inch PMTs. For MCP-PMTs, four afterpulse

**Table 3** The average afterpulse time and charge ratio for each group of afterpulses

PMT model	MCP-PMT				dynode-PMT		
	M0	M1	M2	M3	D0	D1	D2
afterpulse group							
$R_{AP}[\%]$ , LED intensity 1	2.2	1.9	2.5	0.8	0.2	5.3	5.0
$R_{AP}[\%]$ , LED intensity 2	1.9	1.2	0.8	0.6	0.9	7.3	6.5
$R_{AP}[\%]$ , LED intensity 3	1.7	1.6	1.1	0.8	1.1	7.0	6.4
$R_{AP}[\%]$ , average	1.9	1.6	1.8	0.7	0.7	6.5	6.0
$R_{AP}[\%]$ , total	$R_{AP}^{MCP} = 5.7 \pm 1.5$				$R_{AP}^{Dynode} = 13.2 \pm 2.3$		

groups located at 0.9  $\mu\text{s}$ , 3.1  $\mu\text{s}$ , 4.6  $\mu\text{s}$ , and 17.7  $\mu\text{s}$  after the primary pulse were confirmed, with an average total afterpulse charge ratio of  $5.7 \pm 1.5\%$ . For dynode-PMTs, three afterpulse groups located at 1.1  $\mu\text{s}$ , 4.2  $\mu\text{s}$ , and 15.1  $\mu\text{s}$  after the primary pulse were confirmed, with an average total charge ratio of  $13.2 \pm 2.3\%$ . A simplified afterpulse model was constructed to describe the afterpulse time and charge distribution of JUNO 20-inch PMTs, which can benefit the simulation, calibration, and event reconstruction of future JUNO runs.

## References

- Z. Djurcic et al., [JUNO Collaboration], JUNO Conceptual Design Report. (2015). [arXiv:1508.07166](https://arxiv.org/abs/1508.07166) [physics.ins-det]
- F.P. An, G.P. An, Q. An et al., Neutrino physics with JUNO. *J. Phys. G* **43**, 030401 (2016). <https://doi.org/10.1088/0954-3899/43/3/030401>
- JUNO Collaboration, JUNO physics and detector. *Prog. Part. Nucl. Phys.* **123**, 103927 (2022). <https://doi.org/10.1016/j.pnpnp.2021.103927>
- G. Zhu, J. Liu, Q. Wang et al., Ultrasonic positioning system for the calibration of central detector. *Nucl. Sci. Tech.* **30**, 5 (2019). <https://doi.org/10.1007/s41365-018-0530-x>
- C. Yang, Y. Huang, J. Xu et al., Reconstruction of a muon bundle in the JUNO central detector. *Nucl. Sci. Tech.* **33**, 59 (2022). <https://doi.org/10.1007/s41365-022-01049-3>
- Z. Li, Z. Qian, J. He et al., Improvement of machine learning-based vertex reconstruction for large liquid scintillator detectors with multiple types of PMTs. *Nucl. Sci. Tech.* **33**, 93 (2022). <https://doi.org/10.1007/s41365-022-01078-y>
- P. Coates, A theory of afterpulse formation in photomultipliers and the prepulse height distribution. *J. Phys. D Appl. Phys.* **6**, 1862 (1973). <https://doi.org/10.1088/0022-3727/6/16/306>
- N. Akchurin, H. Kim, A study on ion initiated photomultiplier afterpulses. *Nucl. Instrum. Meth. A* **574**, 121 (2007). <https://doi.org/10.1016/j.nima.2007.01.093>
- K. Ma, W. Kang, J. Ahn et al., Time and amplitude of afterpulse measured with a large size photomultiplier tube. *Nucl. Instrum. Meth. A* **629**, 93 (2011). <https://doi.org/10.1016/j.nima.2010.11.095>
- J. Haser, F. Kaether, C. Langbrandtner et al., Afterpulse measurements of R7081 photomultipliers for the Double Chooz experiment. *J. Instrum.* **8**, P04029 (2013). <https://doi.org/10.1088/1748-0221/8/04/P04029>
- X. Zhao, Z. Tang, C. Li et al., Afterpulse measurement for 8-inch candidate PMTs for LHAASO. *J. Instrum.* **11**, T05002 (2016). <https://doi.org/10.1088/1748-0221/11/05/T05002>
- L. Campbell, Afterpulse measurement and correction. *Rev. Sci. Instrum.* **63**, 5794 (1992). <https://doi.org/10.1063/1.1143365>
- W. Luo, T. Yu, M. Chen et al., Generation of bright attosecond x-ray pulse trains via Thomson scattering from laser-plasma accelerators. *Opt. Express* **22**, 32098–32106 (2014). <https://doi.org/10.1364/OE.22.032098>
- Y. Chang, G. Huang, Y. Heng et al., The R & D of the 20 in. MCP-PMTs for JUNO. *Nucl. Instrum. Meth. A* **824**, 143 (2016). <https://doi.org/10.1016/j.nima.2015.10.106>
- H. Zhang, Z. Wang, W. Wang et al., Tested performance of JUNO 20'' PMTs. *J. Phys. Conf. Ser.* **1468**, 012197 (2020). <https://doi.org/10.1088/1742-6596/1468/1/012197>
- L. Chen, J. Tian, C. Liu et al., Optimization of the electron collection efficiency of a large area MCP-PMT for the JUNO experiment. *Nucl. Instrum. Meth. A* **827**, 124 (2016). <https://doi.org/10.1016/j.nima.2016.04.100>
- S.S. Stevens, J.W. Longworth, Late output pulses from fast photomultipliers. *IEEE Trans. Nucl. Sci.* **19**, 356 (1972). <https://doi.org/10.1109/TNS.1972.4326532>
- B. Lubsandorzhev, R. Vasiljev, Y. Vyatchin et al., Photoelectron backscattering in vacuum phototubes. *Nucl. Instrum. Meth. A* **567**, 12 (2006). <https://doi.org/10.1016/j.nima.2006.05.047>
- B. Lubsandorzhev, P. Pokhil, R. Vasiljev et al., Studies of prepulses and late pulses in the 8'' electron tubes series of photomultipliers. *Nucl. Instrum. Meth. A* **442**, 452 (2000). [https://doi.org/10.1016/S0168-9002\(99\)01272-3](https://doi.org/10.1016/S0168-9002(99)01272-3)
- J. Brack, B. Delgado, J. Felde et al., Characterization of the Hamamatsu R11780 12 in. Photomultiplier tube. *Nucl. Instrum. Meth. A* **712**, 162 (2013). <https://doi.org/10.1016/j.nima.2013.02.022>
- J. Wang, N. Anfimov, J. Guo et al., Database system for managing 20,000 20-inch PMTs at JUNO. *Nucl. Sci. Tech.* **33**, 24 (2022). <https://doi.org/10.1007/s41365-022-01009-x>
- N. Anfimov, Large photocathode 20-inch PMT testing methods for the JUNO experiment. *J. Instrum.* **12**, C06017 (2017). <https://doi.org/10.1088/1748-0221/12/06/C06017>
- B. Wonsak, A. Tietzsch, T. Sterr et al., A container-based facility for testing 20''000 20-inch PMTs for JUNO. *J. Instrum.* **16**, T08001 (2021). <https://doi.org/10.1088/1748-0221/16/08/T08001>
- A. Abusleme, T. Adam, S. Ahmad et al., Mass Testing and Characterization of 20-inch PMTs for JUNO. [arXiv:2205.08629](https://arxiv.org/abs/2205.08629) [physics.ins-det]
- Thorlabs, Inc., <https://www.thorlabs.com>. Accessed 20 May (2022)
- T. Hakamata, H. Kume, K. Okano et al., Photomultiplier tubes: basics and applications. Hamamatsu Photonics KK Electron Tube Division. Hamamatsu City (2006). <https://www.hamamatsu.com>. Accessed 20 May (2022)
- Y. Zhang, Z. Wang, M. Li et al., Study of 20-inch PMTs dark count generated large pulses. [arXiv:2206.07456](https://arxiv.org/abs/2206.07456) [physics.ins-det]
- C. Liu, M. Li, Z. Wang et al., Check on the features of potted 20-inch PMTs with 1F3 electronics prototype at Pan-Asia. [arXiv:2208.08264](https://arxiv.org/abs/2208.08264) [physics.ins-det]
- Y. Cheng, S. Qian, Z. Ning et al., The high-speed after-pulse measurement system for PMT. *J. Instrum.* **13**, P05014 (2018). <https://doi.org/10.1088/1748-0221/13/05/P05014>
- S. Aiello, S. Akrame, F. Ameli et al., Characterisation of the Hamamatsu photomultipliers for the KM3NeT Neutrino Telescope. *J. Instrum.* **13**, P05035 (2018). <https://doi.org/10.1088/1748-0221/13/05/P05035>
- U. Akgun, A. Ayan, G. Aydin et al., Afterpulse timing and rate investigation of three different Hamamatsu Photomultiplier Tubes. *J. Instrum.* **3**, T01001 (2008). <https://doi.org/10.1088/1748-0221/3/01/T01001>
- F. Kaether, C. Langbrandtner, Transit time and charge correlations of single photoelectron events in R7081 photomultiplier tubes. *J. Instrum.* **7**, P09002 (2012). <https://doi.org/10.1088/1748-0221/7/09/P09002>
- K. Tudyka, G. Adamiec, A. Bluszcz, Simulation of He<sup>+</sup> induced afterpulses in PMTs. *Rev. Sci. Instrum.* **87**, 063120 (2016). <https://doi.org/10.1063/1.4954511>
- H. Zhang, Z. Wang, F. Luo et al., Gain and charge response of 20'' MCP and dynode PMTs. *J. Instrum.* **16**, T08009 (2021). <https://doi.org/10.1088/1748-0221/16/08/T08009>
- Q. Wu, S. Qian, Y. Cao et al., The status of the 20-inch MCP-PMT and its APR test result. *Nuclear Sci. Symp. Med. Imaging Conf.* **2019**, 1 (2019). <https://doi.org/10.1109/NSS/MIC42101.2019.9059825>
- Q. Wu, S. Qian, L. Ma et al., Study of after-pulses in the 20-inch HQE-MCP-PMT for the JUNO experiment. *Nucl. Instrum. Meth. A* **1003**, 16 (2021). <https://doi.org/10.1016/j.nima.2021.165351>
- P. Amaudruz, M. Batygov, B. Beltran et al., In-situ characterization of the Hamamatsu R5912-HQE photomultiplier tubes used in the

DEAP-3600 experiment. Nucl. Instrum. Meth. A **922**, 373 (2019).  
<https://doi.org/10.1016/j.nima.2018.12.058>

Springer Nature or its licensor (e.g. a society or other partner) holds exclusive rights to this article under a publishing agreement with the

author(s) or other rightsholder(s); author self-archiving of the accepted manuscript version of this article is solely governed by the terms of such publishing agreement and applicable law.